SCIENTIFIC REPORTS

OPEN

SUBJECT AREAS:
BATTERIES
NANOPARTICLES
SOLID-STATE CHEMISTRY
SYNTHESIS AND PROCESSING

Received
13 February 2013

Accepted
6 December 2013

Published
6 January 2014

Correspondence and requests for materials should be addressed to H.P. (huanpangchem@hotmail.com)

Microwave-assisted synthesis of NiS_2 nanostructures for supercapacitors and cocatalytic enhancing photocatalytic H_2 production

Huan Pang[1,2], Chengzhen Wei[1], Xuexue Li[1], Guochang Li[1], Yahui Ma[1], Sujuan Li[1], Jing Chen[1] & Jiangshan Zhang[1]

[1]College of Chemistry and Chemical Engineering, Anyang Normal University, Anyang, Henan 455000, China, [2]State Key Laboratory of Coordination Chemistry, Nanjing University, Nanjing, Jiangsu 210093, China.

Uniform NiS_2 nanocubes are successfully synthesized with a microwave-assisted method. Interestingly, NiS_2 nanocubes, nanospheres and nanoparticles are obtained by controlling microwave reaction time. NiS_2 nanomaterials are primarily applied to supercapacitors and cocatalytic enhancing photocatalytic H_2 production. Different morphologies of NiS_2 nanostructures show different electrochemical and cocatalytic enhancing H_2 production activities. Benefited novel nanostructures, NiS_2 nanocube electrodes show a large specific capacitance (695 F g^{-1} at 1.25 A g^{-1}) and excellent cycling performance (the retention 93.4% of initial specific capacitance after 3000 cycles). More importantly, NiS_2 nanospheres show highly cocatalytic enhancing photocatalytic for H_2 evolution, in which the photocatalytic H_2 production is up to 3400 μmol during 12 hours under irradiation of visible light (λ>420 nm) with an average H_2 production rate of 283 μmol h^{-1}.

Electrochemical capacitors are known by different names, such as ultracapacitors or supercapacitors, and have attracted considerable attention over the past decades owing to their higher power density and longer cycle life than secondary batteries and conventional electrostatic and electrolytic capacitors. In particular, supercapacitors based on ruthenium oxides have shown ultrahigh pseudocapacitance and excellent reversibility. However, the high cost of ruthenium makes this material unsuitable for commercial applications. Hence, searching for alternative and inexpensive electrode materials with good capacitive properties becomes urgent[1–7].

Hydrogen production from photo-induced water splitting has received increasing attention because of its potential in simultaneously solving energy and environmental problems. In order to utilize the abundant solar energy, the development of visible-light active photocatalysts is of great importance. To date, many semiconductor photocatalyst systems have been reported to be active under visible light. Besides metal-oxide semiconductors, efficient photocatalyst systems for hydrogen evolution have been obtained with some sulfide photocatalysts[8–12].

Metal chalcogenide nanomaterials have attracted great attention due to their excellent properties and promising applications in electronic, optical and optoelectronic devices[13,14]. Among the family of metal sulfides, nickel sulfides have attracted much interest not only because the nickel sulfide system contains a number of phases, but also because of their multiple applications as a possible transformation toughened. So, different phases and morphologies of nickel sulfides sometimes coexist. Thus to obtain a uniform morphology with a pure phase of nickel sulfides is still a challenge and has attracted a lot of attention[15–17].

NiS_2, a pyrite structure, has interesting electrical, optical and magnetic properties[18,19]. However, it has been difficult to control the synthesis of uniform NiS_2 micro/nanoparticles due to their natural chemical properties. There are few literature sources on the morphology control synthesis of NiS_2 nanocrystallites[20,21]. Microwave irradiation has been demonstrated for the synthesis of a variety of nanomaterials including metals, metal oxides, chalcogenides, bimetallic alloys and semiconductors with controlled size and shape but without the need for high temperature or high pressure[22–30].

Herein, we have synthesized uniform NiS_2 nanocubes with a microwave-assisted method, and its possible growth mechanism has been further explored. More importantly, NiS_2 nanocubes, nanospheres and

nanoparticles were successfully applied to electrode materials of supercapacitors and cocatalytic enhancing photocatalytic H_2 production. As a result of their novel nanostructures, NiS_2 nanocube electrodes show a large specific capacitance (695 F g^{-1} at 1.25 A g^{-1}) and excellent cycling performance (maintaining 93.4% of initial specific capacitance after 3000 cycles). What's more, the performance of H_2 production indicates the effectively cocatalytic enhancing photocatalytic activity of NiS_2 nanospheres, in which the photocatalytic H_2 production is up to 3400 μmol during 12 hours under irradiation of visible light (λ>420 nm) with an average H_2 production rate of 283 μmol h^{-1}.

Results

A typical XRD pattern of the as-prepared product is displayed in Fig. 1a, showing that the sample has good crystallinity. All diffraction peaks can be clearly indexed to cubic pyrite NiS_2, which is consistent with the reported data for NiS_2 (JCPDS Card File No. 03-0734). A typical low-magnification scanning electron microscopy (SEM) image in Fig. 1b shows that the sample is composed of homogenous nanocubes. It has a diameter of ~200 nm shown in Fig. 1c. The uniform nanocube morphology is further revealed by the transmission electron microscopy (TEM) image shown in Fig. 1d. It further confirms the nanocubed structures. Fig. 1e, f show the high-resolution (HR) TEM image and the selected area electron diffraction (SAED) pattern taken from the individual nanocube shown in Fig. 1d. More interestingly, these results demonstrate the highly crystalline nature of the product. The measured distances of the neighboring lattice fringes in Fig. 1e are 0.23 nm, corresponding well to the (211) lattice spacing.

NiS_2 nanospheres were obtained after 2 hours microwave radiation (Fig. 2). The nanosphere is not uniform as the nanocube, whose size is in range from 50 to 150 nm from Fig. 2a, b and its size-distribution diagram in inset of Fig. 2b. The surface of NiS_2 nanospheres is not smooth (Fig. 2c). These porous, rough surfaces do not only offer high surface areas, but provide small molecular and electrolyte accesses. The crystallization of a individual NiS_2 nanosphere is polycrystalline in Fig. 2d, which is further proved by its corresponding SAED patterns.

To understand possible growth process during the shape evolution of the product, morphologies of the time-dependent products obtained at 150°C were carefully observed, as shown in Supplementary Information Fig. S1. From Fig. S1a, nanoparticles (size <50 nm) were obtained under microwave radiation for 30 minutes. After 2 hours microwave radiation, many nanospheres (50< size < 150 nm) were observed in Fig. S1b. And after 3 hours microwave radiation, NiS_2 nanocubes were successfully synthesized, which might have formed based on the NiS_2 nanospheres (Fig. S1c). There are some formless nanocrystals dispersed among these NiS_2 nanocubes. After microwave radiation for 4 hours, uniform NiS_2 nanocubes were successfully obtained. TEM image of NiS_2 nanoparticles was shown in Fig. S2. Clearly, the size of NiS_2 nanoparticles is <50 nm, which is in accordance with the result shown in Fig. S1. The shape changes of the NiS_2 nanostructures and their morphological evolution is shown in Fig. 3, it is seen that shape changes of the NiS_2 nanostructures have evaluated from formless nanoparticles to nanocubes.

To understand crystallographic evolutions, XRD patterns of samples obtained under different radiation times were measured seen in Fig. S3. Clearly, the NiS_2 phase was successfully obtained after 30 min radiation, but all the peaks were wide and weak which means the crystallinity is not good. The crystallinity has been enhanced by the prolonged radiation time. When we prolonged the radiation time to 3 hours, all the peaks are strong and narrow, which is consistent with NiS_2 (JCPDS Card File No. 03-0734). One notable observation from these XRD patterns is that with the formation of nanocubes from nanoparticles, the intensity of the (200) peak increases drastically compared to those of the other peaks. This exceptionally strong (200) peak for samples (3 hours, and 4 hours radiation time) suggests that the {100} facets of these NiS_2 nanocubes are preferentially oriented parallel to the underlying substrate surface when a monolayer of nanocubes is deposited. Of course, the greater areas of the {100} facets relative to those of the other facets (that is, the {110} and

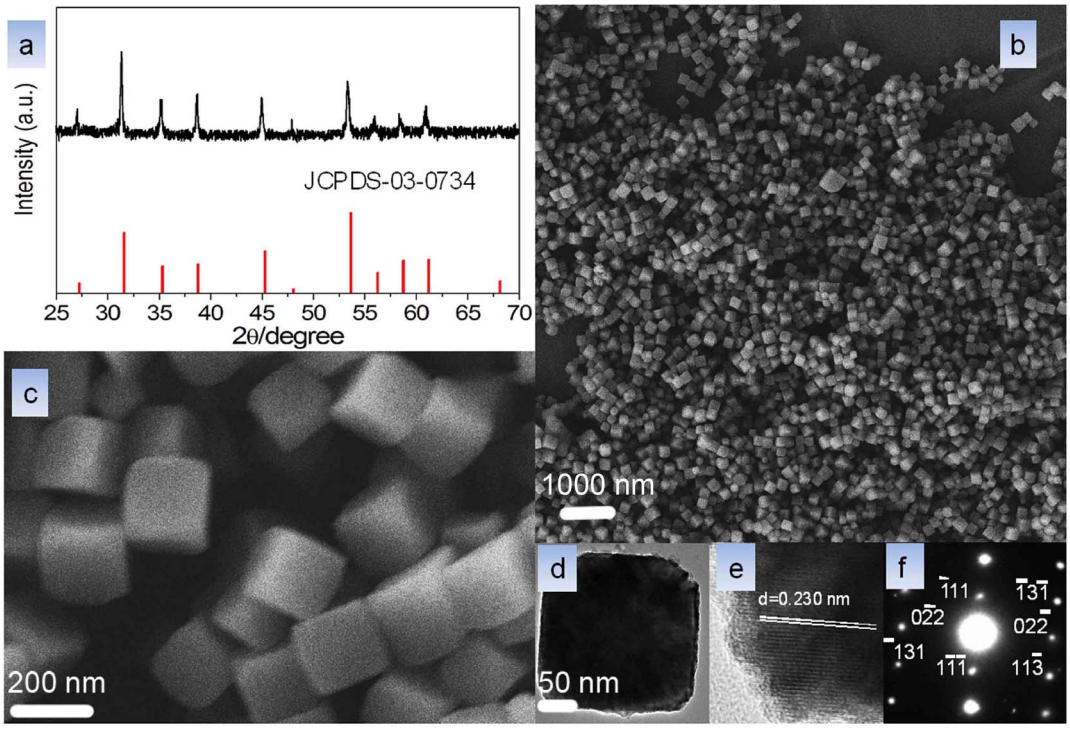

Figure 1 | (a) XRD pattern of NiS_2 nanocubes and JCPDS Card File No. 03-0734-NiS_2, (b, c) SEM images of NiS_2 nanocubes, (d) TEM images of NiS_2 nanocubes, (e) corresponding HRTEM image and (f) corresponding SAED pattern.

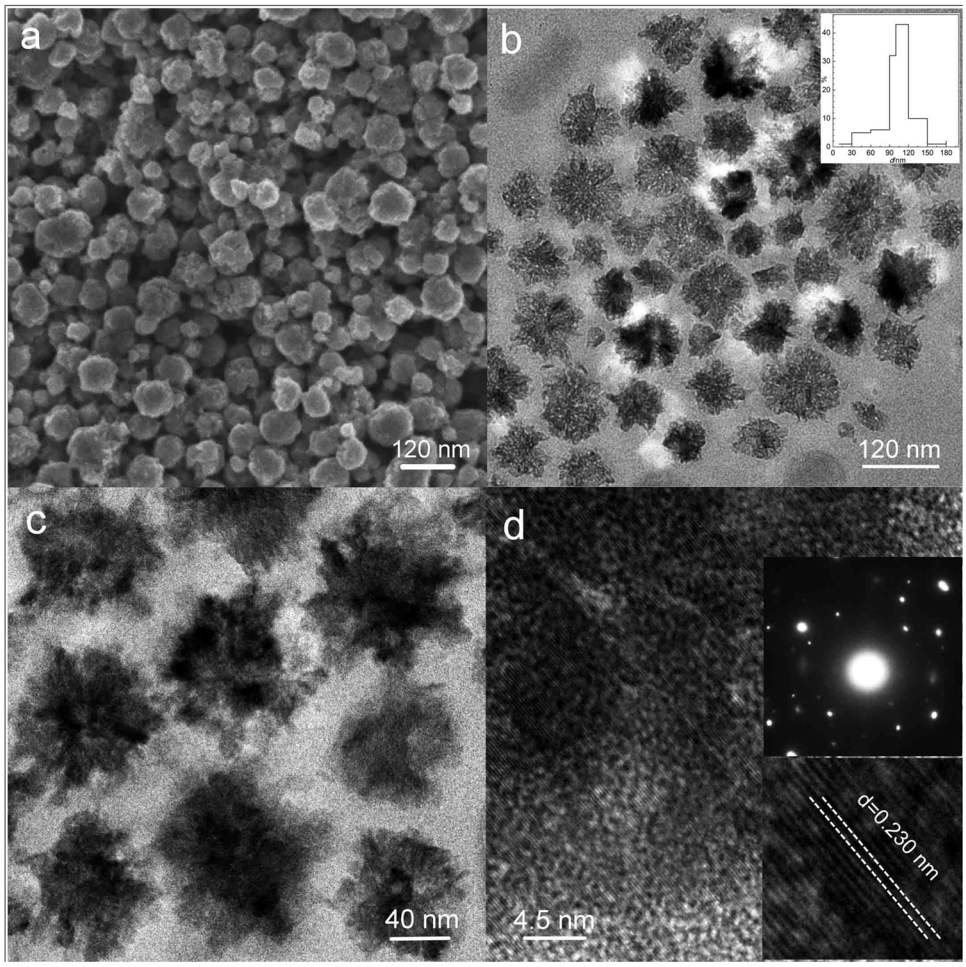

Figure 2 | (a) SEM image of NiS_2 nanospheres, (b, c) TEM images of NiS_2 nanospheres, (d) HRTEM image and SAED patterns, in inset of b, its size-distribution diagram.

{111} facets) for the NiS_2 nanocubes may also contribute significantly to this interesting XRD effect.

To gain further insight into the specific surface area of NiS_2 nanostructures, Brunauer-Emmett-Teller (BET) measurements were performed. And the N_2 adsorption–desorption isotherms of NiS_2 nanomaterials were shown in Fig. S4. BET surface areas of NiS_2 nanocubes, nanospheres and naoparticles are 12.0, 38.3 and 25.1 $m^2\ g^{-1}$ respectively. Different BET surface areas of NiS_2 nanomaterials make different contacts of the electrolyte or water with many surface interfaces of these nanostructures.

Discussion

Cyclic voltammogram (CV) studies were employed to characterize the capacitive performances of the NiS_2 nanocubes. Fig. 4a shows the CVs of the NiS_2 nanocubes electrodes (a mass loading of 5 mg) in 3.0 M KOH electrolyte at different scan rates in the range 5–50 mV s^{-1}. As seen in Fig. 4a, the CVs are almost symmetric, indicating good reversibility of the oxidation and reduction processes. The CVs show a broad redox peak due to faradic reactions of NiS_2 nanocubes, and it indicates that the Faradaic pseudocapacitive property of NiS_2 is based on the surface redox mechanism of Ni^{2+} to Ni^{3+} at the surface. Fig. 5 shows a simple possible route for diffusion of ions and electrons during the electrochemical process. The single nanocrystal, NiS_2 nanocube, shows different diffusion rates of electrons along different crystal planes. And due to the fewer inner crystal interfaces of NiS_2 nanocubes, the diffusion rate of electrons in NiS_2 nanocubes is much quicker than that of polycrystal NiS_2 nanospheres. Moreover, a great number of inner crystal interfaces of NiS_2 nanospheres may cause large inner resistance and contact resistance, which stops electrons from diffusing quickly.

Chronopotentiometry (CP) curves at different current densities are shown in Fig. 4b and Fig. S5. The symmetrical characteristic of

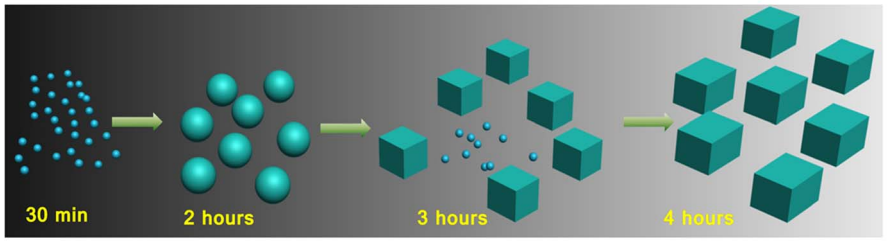

Figure 3 | **Schematic illustration of the shape changes of the NiS_2 nanostructures and their morphological evolution.**

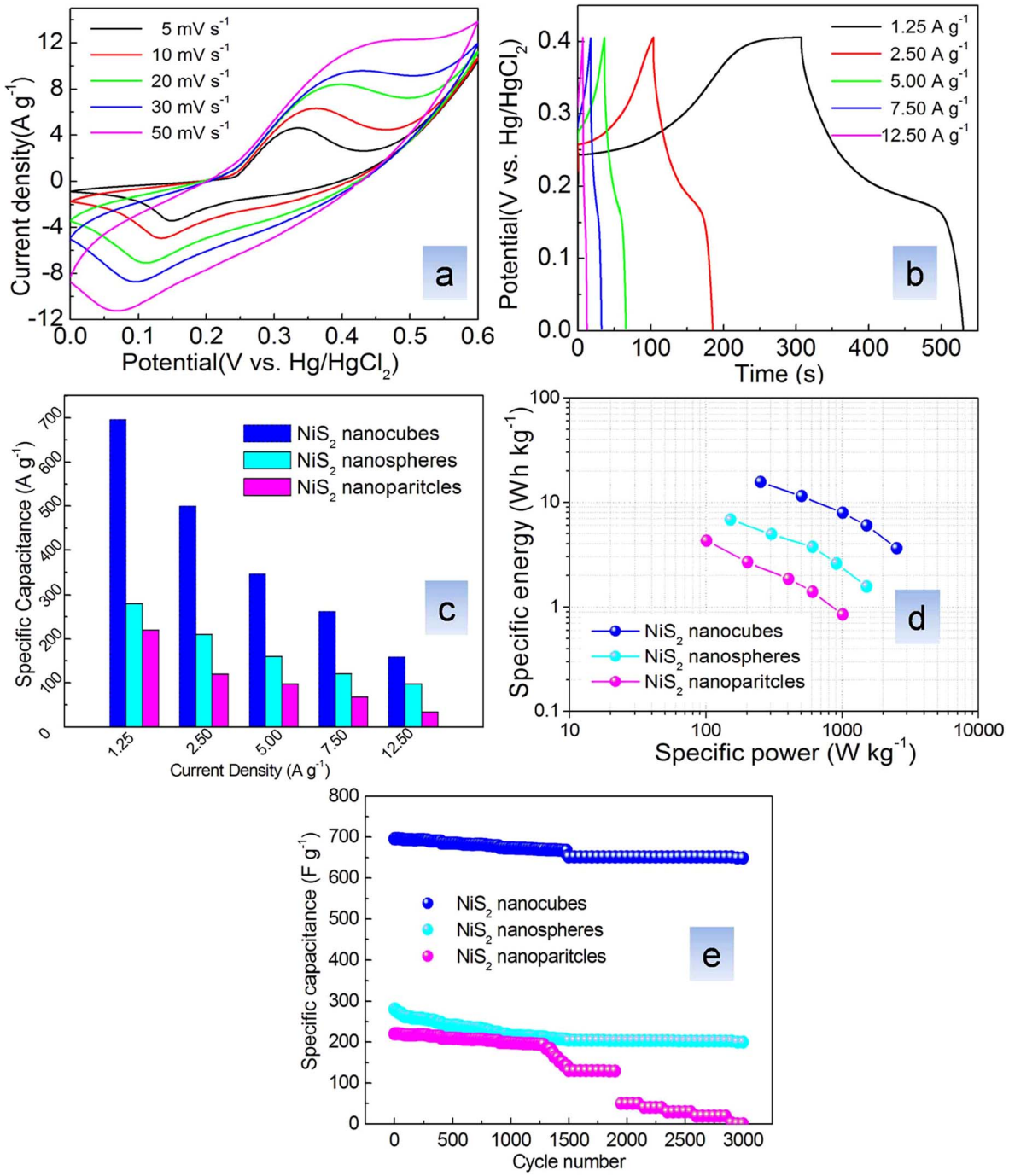

Figure 4 | (a) Cyclic voltammetry experiments within a 0.0–0.60 V range at a scan rate 5, 10, 20, 30 and 50 mV s^{-1} were performed on the NiS_2 nanocube electrodes in 3.0 M KOH electrolytes at room temperature; (b) The galvanostatic charge–discharge curves of NiS_2 nanocube electrodes during current densities were 1.25–12.5 A g^{-1} in 3.0 M KOH electrolytes; (c) Specific capacitances of NiS_2 nanocube, nanosphere, nanoparticle electrodes derived from the discharging curves at the current density of 1.25–12.5 A g^{-1} in 3.0 M KOH electrolytes; (d) Ragone plot of the estimated specific energy and specific power at various charge/discharge rates in 3.0 M KOH electrolytes; (e) Charge/discharge cycling test at the current density of 1.25 A g^{-1} in 3.0 M KOH electrolytes.

charging/discharging curves is good, which means that the NiS_2 nanocube electrodes with excellent electrochemical capability and redox process are reversible. The relationships between the specific capacitances calculated by CP curves and current densities are given in Fig. 4c. Based on the CP curves, NiS_2 nanocube electrodes have the large specific capacitance and reach up to 695 F g^{-1} at a current density of 1.25 A g^{-1} and remain 158 F g^{-1} even 12.5 A g^{-1}, while that of NiS_2 nanoparticle electrodes is 34 F g^{-1} at 12.5 A g^{-1}. The specific capacitance of NiS_2 nanocube is significantly better than some nickel based nanomaterials, such as NiO nanowires (0.5 A g^{-1}, 180 F g^{-1})[31], NiO nanotubes (0.28 A g^{-1}, 47 F g^{-1})[32], Mesoporous NiO (165 F g^{-1})[33], NiO with ordered mesoporous structure (120 F g^{-1})[34], but lower than NiO flowers[35] (1 A g^{-1}, 710 F g^{-1}) and other supercapacitor materials[36,37].

Specific energy and specific power are the two key factors for evaluating the power applications of electrochemical supercapacitors. A good electrochemical supercapacitor is expected to provide both high energy density and specific capacitance. Fig. 4d shows the

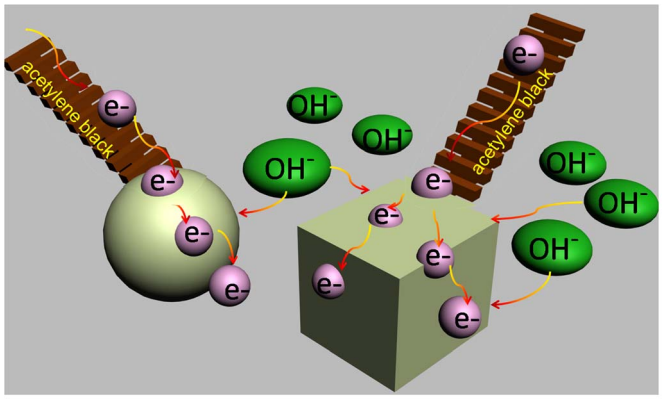

Figure 5 | A simple route for diffusion of ions and electrons during the electrochemical process.

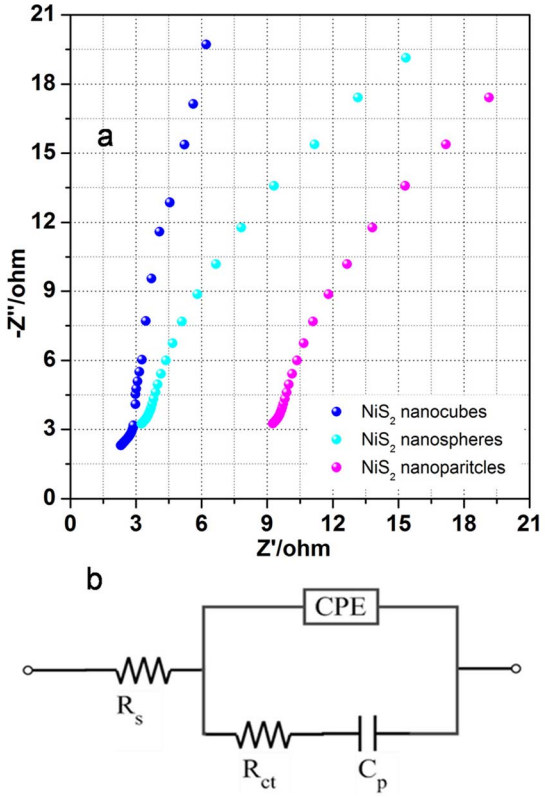

Figure 6 | (a) Electrochemical impedance spectra (EIS) for NiS_2 nanostructured electrodes under room temperature in 3.0 M KOH solutions; (b) An equivalent circuit an consisting of a bulk solution resistance R_s, a charge-transfer R_{ct}, a pseudocapacitive element C_p from redox process of NiS_2 nanomaterials, and a constant phase element (CPE) to account for the double-layer capacitance.

Ragone plot for NiS_2 nanostructured electrodes in 3.0 M KOH aqueous solution. For NiS_2 nanocubes electrodes, it also has well specific energy and specific power. The specific energy of NiS_2 nanocube electrodes decreases from 15.7 to 3.6 Wh kg^{-1}, while the specific power increases from 254 to 2537 W kg^{-1} as the galvanostatic charge/discharge current density increases from 1.25 to 12.5 A g^{-1}. As a comparison, NiS_2 nanoparticle electrodes have very small specific energy (changing from 4.3 to 0.8 Wh kg^{-1}).

It is important for electrode materials to have good specific capacitance retention. Supercapacitors should work steadily and safely, which requires the specific capacitance of electrode materials to change as little as possible. Relationships of the specific capacitance against the cycling number of NiS_2 nanostructured materials are shown in Fig. 4e. It shows its excellent specific capacitance retention under 1.25 A g^{-1}. After 200 continuous charge–discharge cycles, NiS_2 nanocubes electrodes almost retain the same specific capacitance as its initial value. More importantly, NiS_2 nanocubes electrodes still retain more than 93.4% of its specific capacitance after 3000 continuous charge–discharge cycles, while the specific capacitance of NiS_2 nanoparticles has decreased nearly to zero.

To identify the exact electrical conductivity of electrodes, we measured EIS spectrum of NiS_2 nanostructure electrodes at room temperature in the frequency range from 0.01 to 10^5 Hz under open-circuit conditions, which is shown in Fig. 6a. An equivalent circuit used to fit the impedance curve is given in Fig. 6b, which is similar to the circuit employed for the working electrode of supercapacitors. The EIS data can be fitted by a bulk solution resistance R_s, a charge-transfer R_{ct} and a pseudocapacitive element C_p from the redox process of electrode materials, and a CPE to account for the double-layer capacitance. The charge-transfer resistance R_{ct} of all the samples was calculated by ZSimpWin software. And from the calculated results, we found that NiS_2 nanocube electrodes have a lowest value 2.7 Ω. And the detailed R_{ct} values of nanosphere and nanoparticle electrodes are 5.9 Ω and 17.2 Ω respectively. This clearly demonstrates the reduced charge-transfer resistance of the NiS_2 nanocubes electrodes. In addition, the charge-transfer resistance R_{ct}, also called Faraday resistance, is a limiting factor for the specific power of the supercapacitor. It is the low Faraday resistance that results in the high specific power of NiS_2 nanocube electrodes. This cubic structure surface-interface character might also decrease the polarization of the electrode, and thus might increase the capacity.

The as-prepared NiS_2 nanomaterials (nanocubes, nanospheres and nanoparticles) are thus evaluated as a cocatalytic enhancing photocatalyst for H_2 production. Fig. 7 illustrates a possible mechanism of H_2 production on the as-prepared NiS_2 nanomaterials. Photons are captured by the ErY for activation of the electrons from the highest occupied molecular orbital (HOMO) to the lowest unoccupied molecular orbital (LUMO). The activated election is subsequently adopted by the NiS_2 catalyst with suitable Ni 3d and S 3p hybrid orbital. Nickel with a reduced valence state facilitates the proton reduction for the formation of H_2 gas. At the same time, the oxidized ErY is reduced to its ground state by TEOA as the electron donor. Fig. 8 shows the time course of H_2 evolution for different NiS_2 nanomaterials. In our system, in the first 8 hours, 3210 μmol of H_2 gas is generated under the irradiation of visible light ($\lambda > 420$ nm) for the NiS_2 nanospheres, while that of nanocubes and nanoparticles is 1980 and 2220 μmol. More importantly, after 12 hours, the total H_2 gas of NiS_2 nanospheres is up to 3400 μmol with an average H_2 production rate of 283 μmol h^{-1}. A high H_2 production rate of 5.66 mmol h^{-1} g^{-1} and such H_2 production performance is superior to those reported previously[12,38,39]. What is more, an apparent quantum efficiency of 13.6% at 420 nm is measured for NiS_2 nanospheres, while that of NiS_2 nanocubes and nanoparticles is 10.8% and 9.6%. On the contrary, only 1980 μmol (NiS_2 nancubes) and 2220 μmol (NiS_2 nanoparticles) of H_2 gas is collected in 12 hours with an average H_2 production rate of 3.30 (NiS_2 nanocubes) and 3.70 mmol h^{-1} g^{-1} (NiS_2 nanoparticles). This clearly indicates the significantly improved photocatalytic activity of the NiS_2 nanospheres in cocatalytic enhancing photocatalytic H_2 production. The cocatalytic enhancing photocatalytic performance may be related with the active surface of the defect of NiS_2 crystals. Some perfect NiS_2 crystals can improve the transformation of electrons, and the protons are reduced to generate H_2 on some defect NiS_2 crystals which enhances photocatalytic activities.

However, the activity decreases as the irradiation is prolonged, which may be caused by the degradation of the ErY and triethanolamine (TEOA) for this activity loss[40,41]. More importantly, the variation of the reaction mixture solution (ErY in aqueous

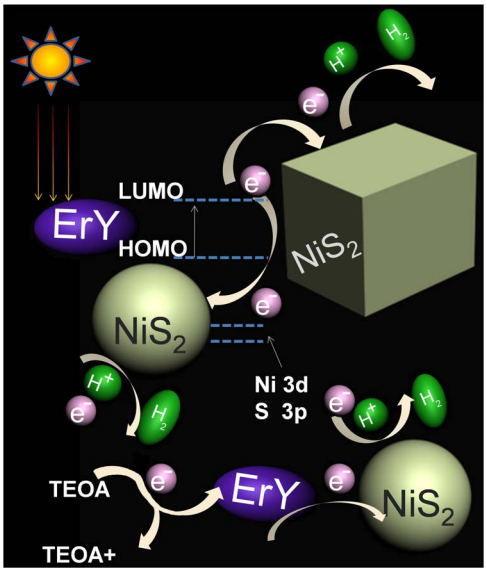

Figure 7 | Schematic illustration of cocatalytic enhancing photocatalytic H_2 production over NiS_2 nanomaterials.

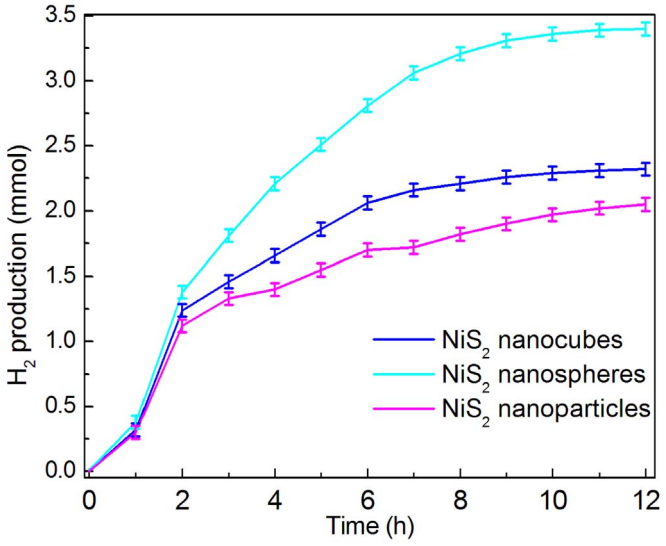

Figure 8 | Time course of cocatalytic enhancing photocatalytic H_2 evolution for as-prepared NiS_2 nanomaterials.

triethanolamine (TEOA) solution) with/without NiS_2 catalyst has been monitored upon irradiation (Figure S6) for proving the above conclusion. The maximum absorption of the reaction mixture solution (ErY in aqueous TEOA solution, pH=8.5) is at around 520 nm. In Figure S6, it is seen that the reaction mixture solution in the presence of NiS_2 is much more stable (Figure S6a) compared to that without the catalyst (Figure S6b). The reaction mixture solution goes through rapid decomposition in the absence of electron acceptor when there is light irradiation. However, the decomposition of the reaction mixture solution with NiS_2 nanostructures exists, and their decomposition rates after the 12 h irradiation are about 38%-NiS_2 nanocubes, 34%-NiS_2 nanospheres and 37%-NiS_2 nanoparticles, respectively.

The inorganic solid catalyst hybrid H_2 production system lies in the recycle ability of the solid catalyst. After the test for 12 h, the NiS_2 nanostructures was collected via a simple centrifugation, and re-dispersed in the same fresh TEOA solution with ErY dye for the second round of testing. As shown in Fig. S7, 2500 μmol of H_2 gas for NiS_2 nanospheres was collected in 12 h, which is over 73.5% of the amount obtained in their first round. That the activity deceased is possibly due to the damage of NiS_2 nanospheres, and the damage of their active surface under long time irradiation. Therefore, SEM images of the 2th circle run as indicated in Figure S7 are shown in Figure S8. NiS_2 nanostructures are still nanocubes, nanospheres and nanoparticles. However, NiS_2 nanocubes are not uniform as the before, the surface of NiS_2 nanospheres becomes smoothly and NiS_2 nanoparticles form some aggregations after prolonged light irradiation. The dropping of activity may be also caused due to the change of NiS_2 morphologies.

This excellent H_2 production performance of the NiS_2 nanospheres may be caused by many factors. NiS_2 nanospheres have rough surfaces with high surface area, which largely facilitates the efficient transfer of photogenerated electrons to improve the photocatalytic efficiency. Ion diffusion and electron transport both play an important role in the performance of supercapacitors and enhancing-cocatalytic photocatalysis. Usually, photocatalytic reaction generally occurs on the surface of nanomaterials. Under such a condition, the electron does not need to diffuse into the inner of these materials. These materials with rough surfaces have large surface area structures, and always show better in cocatalytic enhancing photocatalysis due to effective surface photocatalytic reaction. This might be the reason for the highest cocatalytic enhancing photocatalytic activities of NiS_2 nanospheres with highest surface area, while the cocatalytic enhancing photocatalytic activities of nanoparticles are better than those of nanocubes.

But the resistance, arising from the inherent low electronic conductivity of active materials and the boundary interfaces among active material particles, would much limit the high power performance of supercapacitors. Moreover, the surface reaction of electrode materials largely limits its electrochemical activities. The electronic transport in a nanosized material electrode is shown schematically in Fig. 9, where some carbon additive is employed to improve the conductivity of total electrode. In some cases, small sized nanocrystal materials cannot effectively shorten the path length for electronic transport. Nanoparticles with a very high specific surface area and high surface energy (such as the as-prepared NiS_2 nanoparticles, NiS_2 nanospheres) are difficult to disperse and mix with a carbon additive. Accordingly, the electronic transport length is still very long because only a small number of nanoparticles can directly contact the carbon additive and obtain electrons (such as NiS_2 nanoparticle, nanosphere). Furthermore, the large interface resistance of NiS_2 nanoparticles, and nanospheres still exists, especially when the unit size of the particle is within a typical nano-scale, which is the reason that NiS_2 nanoparticle electrodes and NiS_2 nanosphere electrodes have large R_{ct} and low specific capacitance.

However, different supercapabilities of NiS_2 nanostructured electrodes should be attributed to many different reasons. The most important reason must be associated with easier paths for ions, electrons and electrolytes. The as-prepared single crystal NiS_2 nanocubic structure may have novel surface-interface characters and good electrical conductivity for electrochemical charge-discharge process. These novel chemical-physical characters bring the novel surface-interface and diffusion paths, leading to high electrochemical activities.

In summary, uniform NiS_2 nanocubes have been successfully synthesized through a microwave-assisted method. Different nanostructured NiS_2 samples show different surface-interface conditions, which plays key roles to ion intercalation/extraction and electrolyte accesses. The measurement of electrochemical and cocatalytic enhancing photocatalytic activities of nanostructured NiS_2 materials is important work, which illustrates NiS_2 nanomaterials can be applied as an electroactive material for supercapacitors and the high performance of cocatalytic enhancing photocatalytic H_2 production. Interestingly, the electron transport of NiS_2 nano/microstructures may determine the electrochemical capacitor performance. It means

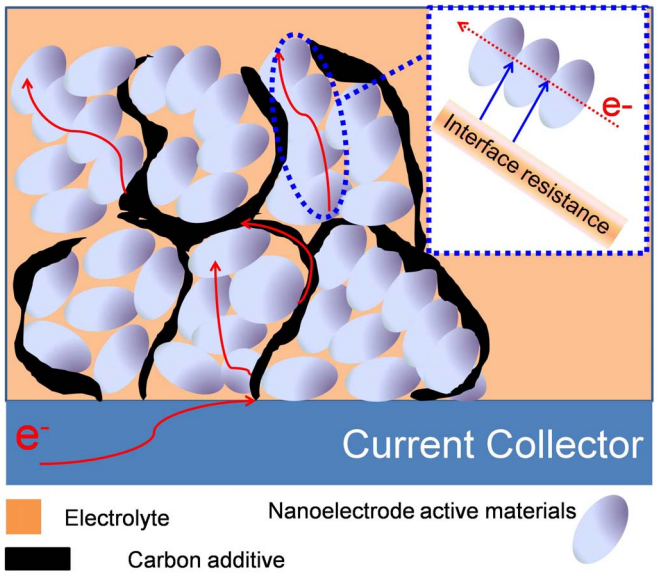

Figure 9 | Schematic representation showing the electronic transport length in nanoparticles based electrode.

that the one which has the good electron transport has effective capacitor performance. What is more, NiS_2 nanospheres with high surface areas are an effective cocatalytic enhancing photocatalyst without noble metal under visible light for photocatalytic H_2 production. It is a good example to prove that the physical and chemical properties of nano/microstructured materials are related with their structures, and the precise control of morphology of nanomaterials will serve for controlling their performance.

Methods

All the samples were prepared in a microwave system (2.45 GHz, 150 W, Discover SP, CEM), which is equipped with in situ magnetic stirring. The exposure time and temperature were programmed. The automatic temperature-control system allowed continuous monitor and control (1°C) of the internal temperature of reaction systems. The preset profile (desired time and temperature) was followed automatically by continuously adjusting the applied microwave power.

Uniform NiS_2 nanocubes. In typical synthesis, 12.0 mL 0.10 M $Ni(NO_3)_2$ solution, 0.40 g sulfourea, 0.30 g Polyvinylpyrrolidone K-30 (PVP) were added into 3.0 mL 0.10 M NaOH solution. After treating the mixture at 150°C for 4 hours under microwave irradiation, the reaction mixture was rapidly cooled to room temperature by an air compressor. The product was collected, washed with deionized water and absolute ethanol, and dried in the air.

Characterizations. The morphology of as-prepared samples was observed by a JEOL JSM-6701F field-emission scanning electron microscope (FE-SEM) at an acceleration voltage of 5.0 kV. The phase analyses of the samples were performed by X-ray diffraction (XRD) on a Rigaku-Ultima III with Cu Kα radiation (λ=1.5418 Å). Nitrogen adsorption-desorption measurements were performed on a Gemini VII 2390 Analyzer at 77 K with the volumetric method. The specific surface area was obtained from the N_2 adsorption-desorption isotherms and was calculated with the Brunauer-Emmett-Teller (BET) method. Transmission electron microscopy (TEM) images and HRTEM images were captured on the JEM-2100 instrument microscopy at an acceleration voltage of 200 kV.

Electrochemical measurement. Electrochemical study on NiS_2 nanostructured electrodes was carried out on a CHI 660D electrochemical working station (Shanghai Chenhua Instrument, Inc.). All electrochemical performances were carried out in a conventional three-electrode system equipped with platinum electrode and a saturated calomel electrode (SCE) as counter and reference electrodes, respectively. Before taking the electrochemical measurement, we have purged out O_2 from the solution by the inert gas Ar. The working electrode was made by mixing active materials (NiS_2 nanomaterials), acetylene black, and PTFE (polytetrafluoroethylene) with a weight ratio of 80 : 15 : 5, coated on a piece of foamed nickel foam of about 1 cm^2, and pressed to be a thin foil at the pressure of 5.0 MPa. The electrolyte was a 3.0 M KOH solution. Cyclic voltammetry and galvanostatic charge–discharge methods were used to investigate capacitive properties of NiS_2 nanostructured electrodes. And electrochemical impedance spectroscopy measurements of all the samples were conducted at open circuit voltage in the frequency range of 100 kHz to 0.01 Hz with AC voltage amplitude of 5 mV by using PARSTAT2273.

Cocatalytic enhancing photocatalytic H_2 production. The method is the same as that in reference 12. Visible light-driven photocatalytic water splitting reaction was conducted in a top window Pyrex cell connected to a closed gas circulation and evacuation system (The intensity of the light employed was 125.8 mW cm^{-2}). In a typical round, 50 mg of catalyst and 200 mg of Erythrosin Yellowish (ErY) are dispersed in 100 mL of triethanolamine aqueous solution (15 v% of TEOA, pH 8.5) under vigorous stir. A 300 W Xenon lamp equipped with a cut-off filter ($\lambda > 420$ nm) was used to provide incident visible light. The temperature of the photoreaction cell was kept between 19 and 20°C by circulating the cooling water. Before the reaction, the system was evacuated and refilled with argon gas for several times to remove the air and finally filled with argon of approximately 30 torr. The produced hydrogen gas is analyzed by an online gas chromatography (Agilent 6890N, TCD detector, argon as carrier gas, 5 Å molecular sieve column). The apparent quantum efficiency (QE) is measured under the same reaction conditions and the lamp is equipped with a band pass filter (Newport, center wavelength 420 nm, band width 10 nm). The reaction solutions are irradiated under $\lambda > 420$ nm for 1 h before switching to band pass filters during the quantum efficiency measurement. The amount of hydrogen produced in the subsequent 4 h was used to calculate the quantum efficiency using the equation below. The number of photons from the radiation source was measured using a silicon photodiode. QE = [(2 × the number of evolved H_2 molecules)/the number of incident photons] × 100%.

1. Li, Q. *et al.* Design and synthesis of MnO_2/Mn/MnO_2 sandwich-structured nanotube arrays with high supercapacitive performance for electrochemical energy-storage. *Nano Lett.* **12**, 3803–3807 (2012).
2. Liu, C., Li, F., Ma, L. P. & Cheng, H. M. Advanced Materials for Energy Storage. *Adv. Mater.* **22**, E28–E62 (2010).
3. Simon, P. & Gogotsi, Y. Materials for electrochemical capacitors. *Nat. Mater.* **7**, 845–854 (2008).
4. Wang, G. P., Zhang, L. & Zhang, J. J. A review of electrode materials for electrochemical supercapacitors. *Chem. Soc. Rev.* **41**, 797–828 (2012).
5. Wang, H. L., Casalongue, H. S., Liang, Y. Y. & Dai, H. J. Ni(OH)$_2$ Nanoplates Grown on Graphene as Advanced Electrochemical Pseudocapacitor Materials. *J. Am. Chem. Soc.* **132**, 7472–7477 (2010).
6. Yuan, L. Y. *et al.* Flexible Solid-State Supercapacitors Based on Carbon Nanoparticles/MnO_2 Nanorods Hybrid Structure. *Acs Nano.* **6**, 656–661 (2012).
7. Guan, C. *et al.* Hybrid structure of cobalt monoxide nanowire @ nickel hydroxidenitrate nanoflake aligned on nickel foam for high-rate supercapacitor. *Energy & Environ. Sci.* **4**, 4496–4499 (2011).
8. Jing, D. & Guo, L. A novel method for the preparation of a highly stable and active CdS photocatalyst with a special surface nanostructure. *J. Phys. Chem. B* **110**, 11139–11145 (2006).
9. Bao, N., Shen, L., Takata, T. & Domen, K. Self-templated synthesis of nanoporous CdS nanostructures for highly efficient photocatalytic hydrogen production under visible light. *Chem. Mater.* **20**, 110–117 (2008).
10. Zhang, W., Wang, Y., Wang, Z., Zhong, Z. & Xu, R. Highly efficient and noble metal-free NiS/CdS photocatalysts for H_2 evolution from lactic acid sacrificial solution under visible light. *Chem. Commun.* **46**, 7631–7633 (2010).
11. Zong, X. *et al.* Enhancement of photocatalytic H_2 evolution on CdS by loading MoS_2 as cocatalyst under visible light irradiation. *J. Am. Chem. Soc.* **130**, 7176–7177 (2008).
12. Zhu, T., Wu, H. B., Wang, Y. B., Xu, R. & (David) Lou, X. W. Formation of 1D hierarchical structures composed of Ni_3S_2 nanosheets on CNTs backbone for supercapacitors and photocatalytic H_2 production. *Adv. Energy Mater.* **2**, 1497–1502 (2012).
13. Gao, M. R., Xu, Y. F., Jiang, J. & Yu, S. H. Nanostructured metal chalcogenides: synthesis, modification, and applications in energy conversion and storage devices. *Chem. Soc. Rev.* DOI: 10.1039/c2cs35310e.
14. Lai, C. H., Lu, M. Y. & Chen, L. J. Metal sulfide nanostructures: synthesis, properties and applications in energy conversion and storage. *J. Mater. Chem.* **22**, 19–30 (2012).
15. Ghezelbash, A., Sigman, M. B. & Korgel, B. A. Solventless synthesis of nickel sulfide nanorods and triangular nanoprisms. *Nano Lett.* **4**, 537–542 (2004).
16. Hu, Y. *et al.* Synthesis of novel nickel sulfide submicrometer hollow spheres. *Adv. Mater.* **15**, 726–729 (2003).
17. Zhang, L. *et al.* A general solution-phase approach to oriented nanostructured films of metal chalcogenides on metal foils: The case of nickel sulfide. *J. Am. Chem. Soc.* **126**, 8116–8117 (2004).
18. Wilson, J. A. Systematics of the breakdown of Mott insulation in binary transition metal compounds, *Adv. Phys.* **21**, 143–149 (1972).
19. Fujimori, A., Mamiya, K. & Mizokawa, T. Resonant photoemission study of pyrite-type NiS_2, CoS_2 and FeS_2, *Phys. Rev. B* **54**, 16329–16332 (1996).
20. Yang, S. L., Yao, H. B., Gao, M. R. & Yu, S. H. Monodisperse cubic pyrite NiS_2 dodecahedrons and microspheres synthesized by a solvothermal process in a mixed solvent: thermal stability and magnetic properties. *CrystEngComm* **11**, 1383–1390 (2009).

21. Stender, C. L. & Odom, T. W. Chemical nanofabrication: a general route to surface-patterned and free-standing transition metal chalcogenide nanostructures. *J. Mater. Chem.* **17**, 1866–1869 (2007).
22. Zhu, Y. J., Wang, W. W., Qi, R. J. & Hu, X. L. Microwave-assisted synthesis of single-crystalline tellurium nanorods and nanowires in ionic liquids. *Angew. Chem., Int. Ed.* **43**, 1410–1414 (2004).
23. Zhang, S. H., Song, Y., Liang, H. & Zeng, M. H. Microwave-assisted synthesis, crystal structure and properties of a disc-like heptanuclear Co (II) cluster and a heterometallic cubanic Co (II) cluster. *CrystEngComm* **11**, 865–872 (2009).
24. Cao, C. Y., Guo, W., Cui, Z. M., Song, W. G. & Cai, W. Microwave-assisted gas/liquid interfacial synthesis of flowerlike NiO hollow nanosphere precursors and their application as supercapacitor electrodes. *J. Mater. Chem.* **21**, 3204–3209 (2011).
25. Meher, S. K., Justin, P. & Rao, G. R. Microwave-mediated synthesis for improved morphology and pseudocapacitance performance of nickel oxide. *ACS Appl. Mater. Interfaces* **3**, 2063–2073 (2011).
26. Xu, L. P. *et al.* 3D flowerlike α-Nickel hydroxide with enhanced electrochemical activity synthesized by microwave-assisted hydrothermal method. *Chem. Mater.* **20**, 308–316 (2008).
27. Panda, A. B., Glaspell, G. P. & El-Shall, M. S. Microwave synthesis of highly aligned ultra narrow semiconductor rods and wires. *J. Am. Chem. Soc.* **128**, 2790–2791 (2006).
28. Washington II, A. L. & Strouse, G. F. Microwave synthesis of CdSe and CdTe nanocrystals in nonabsorbing alkanes. *J. Am. Chem. Soc.* **130**, 8916–8922 (2008).
29. Hu, B., Wang, S.-B., Wang, K., Zhang, M. & Yu, S.-H. Microwave-assisted rapid facile "green" synthesis of uniform silver nanoparticles: Self-assembly into multilayered films and their optical properties. *J. Phys. Chem. C* **112**, 11169–11174 (2008).
30. Hu, X., Yu, J. C., Gong, J. & Li, Q. Rapid mass production of hierarchically porous $ZnIn_2S_4$ submicrospheres via a microwave-solvothermal process. *Cryst. Growth Des.* **7**, 2444–2448 (2007).
31. Pang, H., Lu, Q. Y., Zhang, Y. Z., Li, Y. C. & Gao, F. Selective synthesis of nickel oxide nanowires and length effect on their electrochemical properties. *Nanoscale* **2**, 920–922 (2010).
32. Pang, H., Lu, Q. Y., Li, Y. C. & Gao, F. Facile synthesis of nickel oxide nanotubes and their antibacterial, electrochemical and magnetic properties. *Chem. Commun.* 7542–7544 (2009).
33. Wang, Y. G. & Xia, Y. Y. Electrochemical capacitance characterization of NiO with ordered mesoporous structure synthesized by template SBA-15. *Electrochimica Acta* **51**, 3223–3227 (2006).
34. Yu, C. *et al.* A simple template-free strategy to synthesize nanoporous manganese and nickel oxides with narrow pore size distribution, and their electrochemical properties. *Adv. Funct. Mater.* **18**, 1544–1554 (2008).
35. Yuan, C. Z., Zhang, X. G., Su, L. H., Gao, B. & Shen, L. F. Facile synthesis and self-assembly of hierarchical porous NiO nano/micro spherical superstructures for high performance supercapacitors. *J. Mater. Chem.* **19**, 5772–5777 (2009).
36. Lu, Z., Chang, Z., Zhu, W. & Sun, X. M. Beta-phased $Ni(OH)_2$ nanowall film with reversible capacitance higher than theoretical Faradic capacitance. *Chem. Commun.* **47**, 9651–9653 (2011).
37. Qu, B. *et al.* β-Cobalt sulfide nanoparticles decorated graphene composite electrodes for high capacity and power supercapacitors, *Nanoscale* **4**, 7810–7816 (2012).
38. Peng, T. Y., Zeng, P., Ke, D. N., Liu, X. J. & Zhang, X. H. Hydrothermal preparation of multiwalled carbon nanotubes (MWCNTs)/CdS nanocomposite and its efficient photocatalytic hydrogen production under visible light irradiation. *Energy Fuels* **25**, 2203–2210 (2011).
39. Li, Q. Y., Chen, L. A. & Lu, G. X. Visible-light-induced photocatalytic hydrogen generation on dye-sensitized multiwalled carbon nanotube/Pt catalyst. *J. Phys. Chem. C* **111**, 11494–11499 (2007).
40. Zhang, W. & Xu, R. Hybrid photocatalytic H_2 evolution systems containing xanthene dyes and inorganic nickel based catalysts Int. *J. Hydrogen Energy* **37**, 17899–17909 (2012).
41. Han, J. *et al.* Nickel-complexes with a mixed-donor ligand for photocatalytic hydrogen evolution from aqueous solutions under visible light. *RSC Advances* **2**, 8293–8296 (2012).

Acknowledgments

This work is supported by the Program for New Century Excellent Talents from the ministry of education (NCET-13-0645) and National Natural Science Foundation of China (NSFC-21201010, 21003001 and 21071006), the Science & Technology Foundation of Henan Province (122102210253, 13A150019), and China Postdoctoral Science Foundation (2012M521115).

Author contributions

H.P., J.S.Z., J.C., S.J.L. and C.Z.W. conceived and designed the experiments. H.P., X.X.L., G.C.L. and Y.H.M. analyzed the measurements. H.P. wrote the manuscript in collaboration with all the authors.

Additional information

Supplementary information accompanies this paper at http://www.nature.com/scientificreports

Competing financial interests: The authors declare no competing financial interests.

How to cite this article: Pang, H. *et al.* Microwave-assisted synthesis of NiS_2 nanostructures for supercapacitors and cocatalytic enhancing photocatalytic H_2 production. *Sci. Rep.* **4**, 3577; DOI:10.1038/srep03577 (2014).